NUMERICAL SIMULATION OF WAVE INTERACTING WITH A SUBMARINE OUTFALL USING IH-2VOF

J. Inverno[1], M. G. Neves[2] and E. Didier[1,2]

Abstract

IH-2VOF numerical model is applied to study wave interacting with a circular cylinder with a diameter of 0.02 m in a water depth of 0.27 m, with a wave period of 1.08 s and a wave height of 0.047 m. The study includes analyses of convergence with the mesh discretization. The convergence of forces, velocities and Keulengan-Carpenter number was obtained when 32 cells were used to define the cylinder.

The influence of the wall proximity on the forces was also analyzed and 15 different ratios between the pipe distance from the bottom and the pipe diameter were simulated, varying from 0.0625 to 1.5. Results of lift, drag and inertia coefficients are compared with the experimental results of the experimental study of Jarno-Druaux et al. (1995) and the same trend in the variation with the gap between the cylinder and the bottom was obtained with the model giving slightly larger values.

1. Introduction

Worldwide, the use of submarine outfalls has been increasing rapidly. Reported accidents with such installations, including accidents in Portugal (Reis and Neves, 2003), have highlighted that their good working conditions are of mandatory importance to the environment, welfare of populations and economy, with accidents being described as having very high environmental, economical and social consequences. Although the science and technology for the design and construction of outfalls has advanced significantly in the last 30 years, major questions still remain unanswered, including the considerable shortcoming in the knowledge of forces induced by waves in submarine outfalls.

For simple horizontal cylindrical pipes, many researchers have conducted two-dimensional (2D) experimental tests and, recently, also some numerical simulations, to study forces, with regular and irregular waves (*e.g.*, Sumer and Fredsoe, 2006; Aristodemo *et al.*, 2010). The influence on hydrodynamic forces for different ratios between the pipe distance from the bottom and the pipe diameter, *e/D*, was also extensively studied in 2D experiments (*e.g.*, Jarno-Druaux *et al.*, 1995), since different *e/D* alters the magnitude and direction of forces on the cylinder.

The IH-2VOF numerical model (Lara *et al.*, 2006) was extensively validated for studies of wave interacting with breakwaters. This model simulates very well the wave generation and propagation, crucial for the determination of forces on submarine outfalls. However, it was not validated for studying the interaction between waves and submarine outfalls.

In order to validate the application of IH-2VOF for wave interacting with submarine outfalls, the model is here applied to the experimental study presented in Jarno-Druaux *et al.* (1995). The study includes analyses of convergence with the mesh discretization and results of the lift, drag and inertia coefficients are compared with the experimental results.

Although this work has been done in the context of outfalls, all scientific concepts here presented are also applicable to other type of marine structures also placed near the sea bottom, as gas and crude oil pipelines.

[1] FCT, Universidade Nova de Lisboa, 2829-516, Monte de Caparica, Portugal. j.inverno@gmail.com

[2] LNEC – National Laboratory for Civil Engineering, Av. do Brasil, 101, 1700-066 Lisbon, Portugal. gneves@lnec.pt, edider@lnec.pt

2. Case study

The case study is a submarine outfall, here represented by a circular cylinder with an external diameter of 0.02 m in a flume with a water depth, *h*, of 0.27 m, following the characteristics of the experimental work described in Jarno-Druaux *et al*. (1995).

The experimental work was carried out in a wave flume 9 m long, 0.8 m wide and 1 m high. Different ratios between the pipe distance from the bottom, *e*, and the pipe diameter, *D*, were tested experimentally, varying from 0.04 to 1.5.

The test were conducted with regular wave conditions with a wave period, *T*, of 1.08 s and a wave height, *H*, of 0.047 m which corresponds to a Reynold number, *Re*=1800 and a Keulengan-Carpenter number, *KC*=4.90.

The experimental results presented in the paper consists essentially on the variation of drag, inertia and lift coefficients with respect to the gap-to diameter ratio, *e*/*D*. The coefficients were calculated based on the measured in-line and transverse forces acting on the cylinder. The drag (C_D) and inertia (C_M) coefficients were calculated through the use of Morison´s equation and a Fourier analysis. Two lift coefficients were determined from the transverse force, corresponding to the maximum lift directed away from (C_L^+) and toward (C_L^-) the wall bottom in the wave period.

Flow velocity was measured during the experiments giving the maximum velocity of the undisturbed flow, U_m, i.e., the velocity at the cylinder axis position in the absence of the cylinder.

For experimental flow visualization, dye was injected into the flow by a thin hole in the cylinder and the emission lines were video recorded.

3. Numerical model

By taking the volume-average of RANS equations, Lin &Liu (1998) presented a two-dimensional numerical model, nicknamed COBRAS, to describe the flow inside and outside maritime structures including permeable layers. Hsu *et al*. (2004) extended the preliminary model by including a set of volume-averaged *k*-ε turbulence balance equations. The movement of the free surface is tracked by the Volume of Fluid (VOF) method.

IH-2VOF is a version of the model COBRAS developed at the University of Cantabria to overcome some of the initial limitations and especially to convert it into a tool for practical application. Most of these modifications have been based on the extensive validation work carried out with the model for low-crested structures and for wave breaking on permeable slopes (Lara *et al*., 2006; Losada *et al*., 2008). The improvements cover the wave generation process and code updating; optimization and improvement of the main subroutines; improvement of input and output data definition; and the development of a graphical user interface and output data processing programs.

In this study, IH-2VOF will be used mainly to calculate the pressure around the cylinder, the velocity field resulting from the interaction of the waves with the cylinder and the vorticity resulting from the wave-structure interaction.

4. Numerical results

4.1. Numerical simulations

Numerical simulations were carried out for a water depth, *h*=0.27 m, a wave period, *T*, of 1.08 s and a wave height, *H*, of 0.047 m, corresponding to the conditions used in the referred experimental work of Jarno-Druaux.

The numerical flume has 3 m long (including at least one wave length before and after the structure, located in the middle of the numerical flume) and 0.33 m high. The computational mesh (Figure 1) was divided in three horizontal regions with different resolutions, corresponding to the wave generation zone (first zone – Zx1), the cylinder vicinity (second zone – Zx2) and the last part of the flume (third zone – Zx3). The grid was non-uniform in the x-direction in the Zx1 and Zx3,

with a minimum cell width close to the Zx2 and a maximum cell width at the boundaries. In the y-direction, the grid was non-uniform from the surface elevation until the cylinder vicinity (Zy2). In the cylinder vicinity (Zx2, Zy2), where the grid is uniform both in the x and in the y directions, the cell width, *dx*, and the cell height, *dy*, was determined based on convergence study (see 4.2).

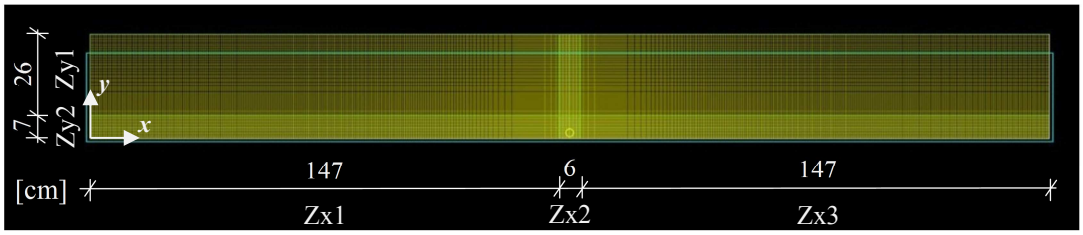

Figure 1. Aspect of the computational grid and corresponding dimensions of the flume

The cylinder was adapted to a rectangular grid and the resulting diameter was verified in order to have the same diameter of the experimental tests in all simulations. Simulations were made varying the cylinder position in y-direction, i.e., with different gap-to diameter ratio. For each pipe position a different mesh was used, maintaining the same grid dimension in the cylinder vicinity.

The pressure obtained from the model is post processed to obtain ensemble time-series of pressure around the structure and the dynamic pressure was calculated by subtracting to these values the static pressure. Integrating the dynamic pressure along the cylinder, the forces are obtained. Based on those forces, the lift, drag and inertia coefficients are calculated with the same methods of the experimental study. For post processing the model results it were used MATLAB programs developed by the authors (Inverno, 2013).

The free surface elevation and the velocity are also analyzed to characterize the flow around the structure. The free surface elevations were obtained at seven numerical gauges (G1 to G7), positioned with a distance of 0.5 m between gauges. The first gauge was positioned at the left boundary, where the wave is generated. The velocity field was analyzed at an undisturbed region (G3).

4.2. Sensitivity analysis of the grid dimension

A convergence study with resolution is firstly performed in order to define the best grid dimension in the vicinity of the cylinder, i.e., the number of cells necessary to obtain a good compromise between computational time and accuracy of the results. This study was made for e/D=0.5. The sensitivity runs consisted essentially on changing the dimension of the horizontal and vertical grid dimension around the cylinder in the zones Sx2 and Sy2 where $dx = dy$. Table 1 shows the characteristics of the six computational domains used in the convergence study of the solution: number of cells, *nc*, number of cells used to define the cylinder diameter, *ncd* /*D*, and the approximately run duration, in days. The runs were performed on a computer with the following specifications: Intel® Core ™ i7 CPU 2.93GHz and 6 GB RAM.

Table 1. Number of cels and run time used for the convergence study

Run	*nc*	*ncd* /*D*	run time (days)
v10_0.50	166815	10	0.5
v20_0.50	300591	20	2.0
v32_0.50	425759	32	4.5
v40_0.50	498721	40	7.0
v50_0.50	584391	50	12.5
v64_0.50	700650	64	24

For each run, several parameters were calculated and compared: U_m, Re, KC, maximum in-line force, divided in forces with the direction of wave propagation, Fx_{max}, and with the opposite direction, Fx_{min}, and maximum transverse force, divided in forces directed away from the bottom wall, F_L^+, and toward the bottom wall, F_L^-. Figure 2 shows the results obtained for KC, U_m, Fx_{min} and F_L^-. Table 2 presents the value of the forces and the correspondent relative variation, $V_{v64\_0.50,}$ using the larger grid, v64_0.50, as the reference value. Fx_{max}, Fx_{min}, F_L^+ and F_L^- were obtained by an averaged of the force obtained for each of 50 waves (from 38.9 s to 92.9 s of the simulation).

Table 2. Results from the convergence study and relative variation referred to v64_0.50 run

Run	Fx_{max} (N/m)	$V_{v64\_0.50}$ (%)	Fx_{min} (N/m)	$V_{v64\_0.50}$ (%)	F_L^+ (N/m)	$V_{v64\_0.50}$ (%)	F_L^- (N/m)	$V_{v64\_0.50}$ (%)
v10_0.50	0.514	40.83	-0.499	43.46	0.218	8.20	-0.240	5.48
v20_0.50	0.427	16.89	-0.422	21.50	0.160	20.69	-0.221	12.93
v32_0.50	0.400	9.70	-0.387	11.32	0.183	9.17	-0.229	9.78
v40_0.50	0.380	4.18	-0.353	1.50	0.202	0.21	-0.235	7.64
v50_0.50	0.368	0.95	-0.356	2.43	0.198	2.08	-0.253	0.55
v64_0.50	0.365	0.00	-0.348	0.00	0.202	0.00	-0.254	0.00

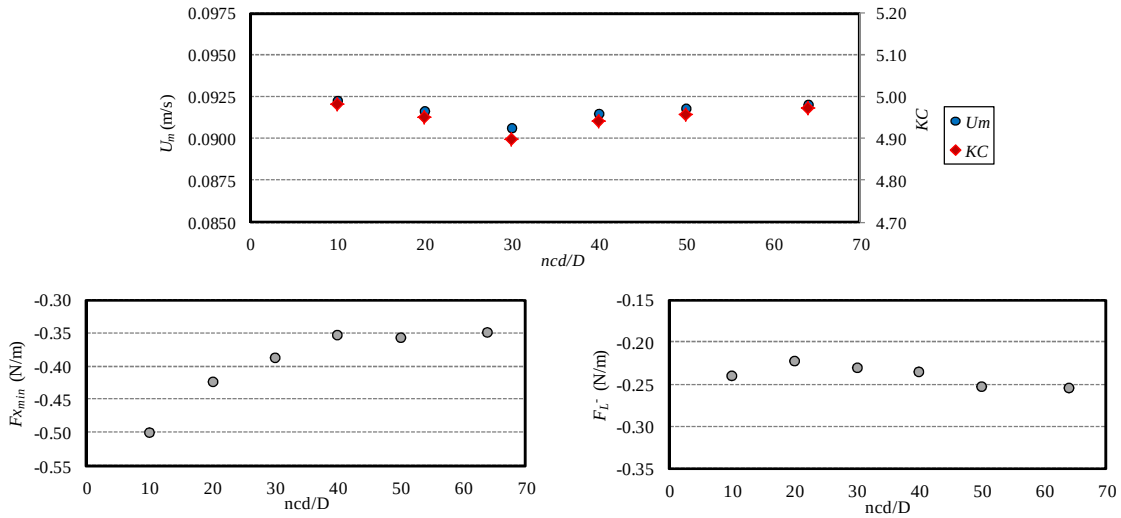

Figure 2. Convergence study results of U_m, KC, Fx_{min} and F_L^-

Analyzing the results presented above, convergence of velocity, KC and forces are obtained for the four finer resolutions. In fact, with the exception of the simulation with the two coarser meshes (v10_0.50 and v20_0.50), the results are very similar, presenting differences from the more refined mesh simulation less than 12% for the in-line forces and less than 10% for the transverse forces. Moreover, for simulation v32_0.50 KC was equal to 4.90, which corresponds exactly to the value obtained in experimental measurements.

Based on these results, the grid dimension chosen for the simulations was the coarser for which convergence was obtained, corresponding to the case of 32 cells for cylinder diameter (v32_0.50).

4.3. Forces in the cylinder

To study the influence of the wall proximity in the cylinder forces, numerical simulations were carried out for 15 cases with the gap-to diameter ratio varying from 0.0625 to 1.5. The distance between the pipe and the bottom was always a multiple of the grid dimension in the cylinder

vicinity (Sx2 and Sy2) where *dx*=*dy*=0.0625 cm.

In order to illustrate the model results, Figure 3 shows the time series of the free surface elevation aligned with the center of the cylinder, $\eta cylinder$, and the correspondent in-line force, *Fx*, and lift force, *FL*, obtained for *e/D*=0.5 between 55.1 s and 60.5 s of simulation. Notice that *Fx* has the same period as the wave but with a different phase. As a feature of an oscillatory flow *Fx* values oscillates between positive (Fx^+) and negative (Fx^-) with a maximum value of Fx^- 6% smaller than Fx^+. The lift force period is approximately half of the wave's period and its value have a more irregular trend than *Fx* because of major influence of the formation and shedding of vortex.

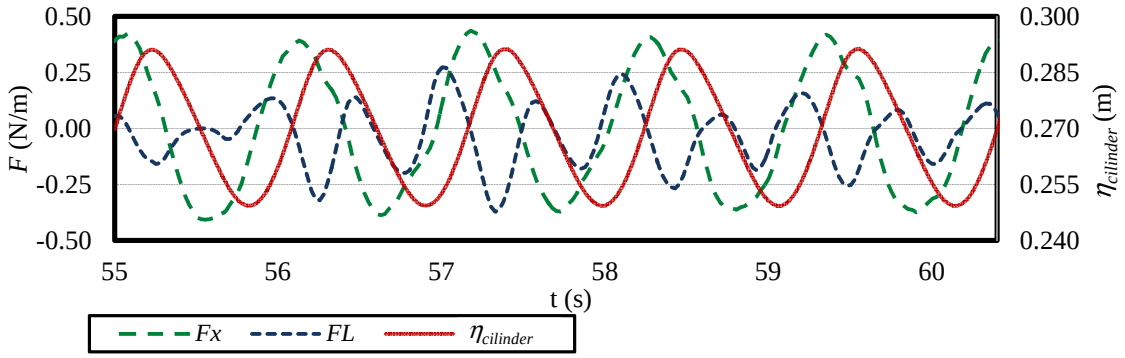

Figure 3. Time series of the surface elevation, in-line forces and lift forces obtained for *e/D*=0.50

The results obtained from the model are used to calculate the in-line and transversal forces and the drag, inertia and lift coefficients. In order to compare with the experimental results presented by Jarno-Druaux *et al*. (1995), dimensionless force coefficients are here calculated as in the experimental results.

For the drag, C_D, and inertia coefficient, C_M, Morison equation and a Fourier analysis using Equations (1) and (2), respectively, are considered.

$$C_D = \frac{1.5\,\pi}{T} \sum_{0}^{T} \frac{Fx(t)\,u(t)}{\rho\,D\,{U_m}^3}\,dt \tag{1}$$

$$C_M = \frac{2\mathrm{KC}}{\pi^3} \sum_{0}^{T} \frac{Fx(t)\,\dot{u}(t)}{\rho\,D\,{U_m}^3}\,dt \tag{2}$$

where *u(t)* and $\dot{u}(t)$ are, respectively, the instantaneous velocity and acceleration and *dt* is the time interval where each parameter was saved from the numerical model simulations.

For the lift coefficient, lift forces (F_L^+ and F_L^-) were normalized by $0.5\rho DLU_m$. Here ρ represents water density and *L* is the length of the cylinder (considered as a unit value). The lift coefficient was divided in maximum lift away from (C_L^+) and toward the bottom wall (C_L^-).

As it was done in the experimental results, in this study C_D and C_M (Figures 4 and 6) were obtained considering an average value for 15 waves (between 55.096 s and 60.496 s). For the same 15 waves it was considered an average value of the maximum C_L^+ and the minimum C_L^- (Figures 7 and 8).

The variation of the drag coefficient with the gap-to-diameter, *e/D*, calculated from the model, *CD_IH-2VOF*, and measured experimentally, *CD_experimental*, is presented in Figure 4. Two lines are also presented to make easy to compare the results trend.

Figure 4 shows that, until certain value of *e/D*, the drag coefficient increase with increasing gap. This *e/D* value varies for experimental (0.20) to numerical results (0.125). For the smallest values of *e/D* the drag coefficient variation is similar to the one observed in steady flows and the decrease

in the values for smallest *e/D* is attributed to the immersion of the cylinder in the boundary layer flow (Jarno-Druaux *et al*., 1995). Taking this into account, it was analyzed if the differences on the value of *e/D* where the maximum of C_D is achieved could be due to differences in the boundary layer. For that, the horizontal velocity profile in a non–perturbed area is compared with the experimental values obtained at the crest and at the trough of the wave (Figure 5). Figure 5 shows that the numerical velocity profile agrees well at the crest and present slightly larger values at the trough (differing less than 13%), when comparing to the experimental velocities, leading to a conclusion that the differences between numerical and experimental results in the boundary layer at the bottom are not significant. However, the effect of both cylinder and bottom boundary layer could be significant and explain the differences observed in the C_D but there are no experimental data available for comparison.

After that maximum value of C_D both numerical and experimental results show a rapid decrease of the drag coefficient until *e/D*=0.75. In this range (0.20<*e/D*<0.75) the numerical and experimental trend is the same and for all simulated cases the numerical results are larger than the experimental ones, with differences around 30%. After *e/D*=0.75, C_D values remain approximately constant because the influence of the wall on the forces are almost negligible; the numerical and experimental trend remains similar although the difference between them increases up to 70%. This significant difference could possibly be due to differences on wave height above the cylinder in the experimental and numerical tests, since the wave height affects the hydrodynamic forces on the cylinder. In the numerical tests the average wave height above the cylinder was 11% smaller than the input wave height (0.047 m). This 11% difference happened due to small wave reflection on the right boundary of the numerical flume. Nonetheless is not possible to determine if this is the reason of this difference because there is no experimental data available for comparison.

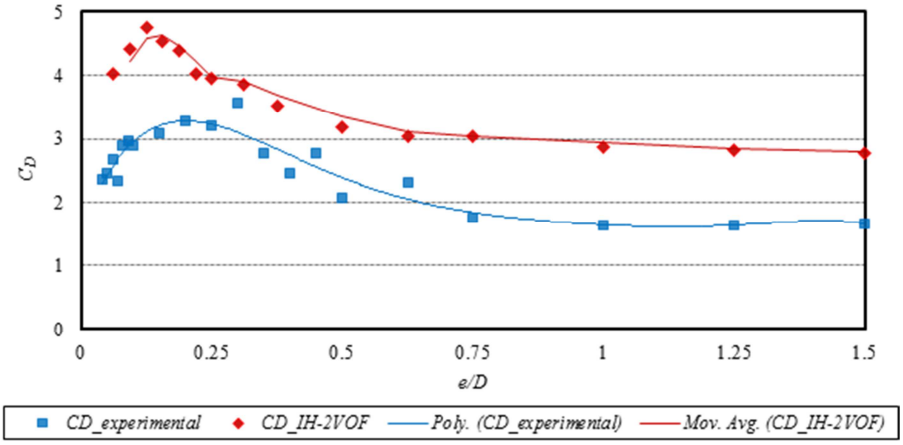

Figure 4. Variation of drag coefficient with the gap-to-diameter: experimental and numerical results

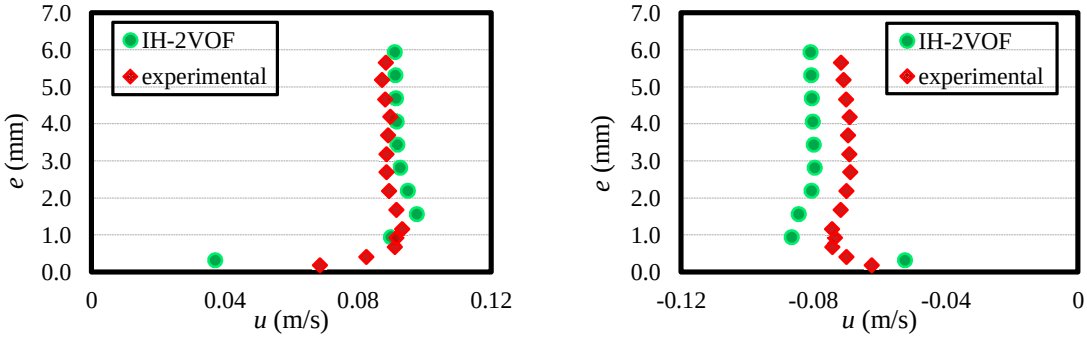

Figure 5. Horizontal velocity profile in a non–perturbed area obtained at the crest (left) and at the through (right) of the wave

The variation of the inertia coefficient with the gap-to-diameter, *e/D*, calculated from the numerical model, *CM_IH-2VOF*, and measured experimentally, *CM_experimental*, is presented in Figure 6. Trend lines are also presented to make easy results comparison.

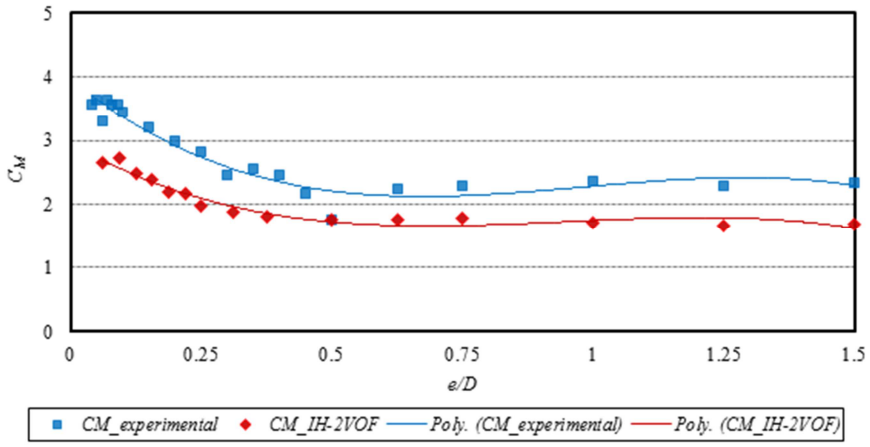

Figure 6. Variation of inertia coefficient with the gap-to-diameter: experimental and numerical results

Figure 6 shows that the trend of variation obtained with the model is similar to the one observed in the experimental tests, with the model giving values 25% larger for all cases. As for the drag coefficient, the maximum C_M is obtained for different values of *e/D*: around 0.05 for experimental and around 0.094 for numerical results. With increasing the gap until *e/D*=0.5 both experimental and numerical results show a decrease of the inertia coefficient and after that value the same trend is also obtained. For a gap larger than *e/D*=1 the inertia coefficient does not change with the increasing of the gap, i.e., is no longer affected by the presence of the wall.

The variation of the lift coefficient with the gap-to-diameter, *e/D*, calculated from the numerical model, CL^+*_IH-2VOF* and CL^-*_IH-2VOF,* and based on the measured experimental values, CL^+*_experimental* and CL^-*_experimental*, respectively lift coefficient directed away from and toward the wall bottom , are presented in Figures 7 and 8. Trend lines are also added to make easy results comparison.

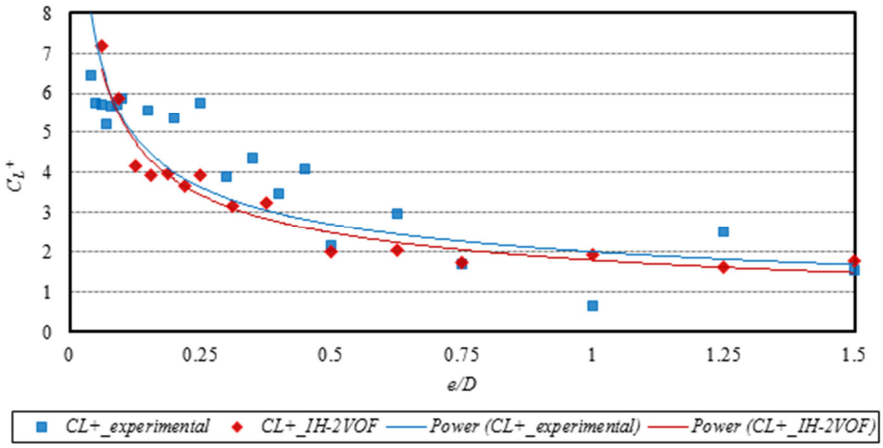

Figure 7. Variation of lift coefficient directed away from the wall bottom with the gap-to-diameter: experimental and numerical results

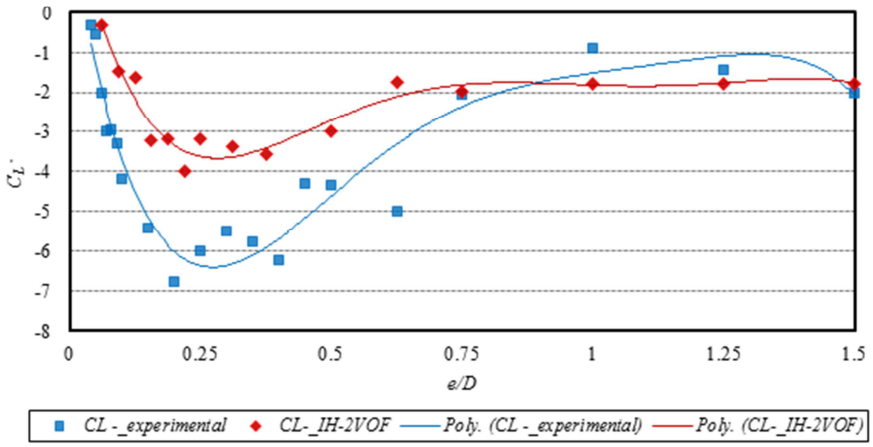

Figure 8. Variation of lift coefficient directed toward the wall bottom with the gap-to-diameter: experimental and numerical results

Figure 7 shows that the trend of variation obtained with the model is similar to the one observed in the experimental tests, with differences around 10% for C_L^+. For C_L^- (Figure 8) differences go up to 30% but experimental and numeric trend is very similar with the same inflection points and similar concavities, although for the numeric case the concavities are smoother. The critical value of *e/D* for which the lift forces acting on the cylinder towards the wall are maximum, are similar for numerical and experimental tests and around 0.25. For the lift coefficients directed away from the wall, C_L^+, as small as the *e/D* gets higher this adimensional force component gets.

For C_L^- differences on the trend are more noticeable, with the numerical model results showing a smaller decrease until *e/D* around 0.25 and a smoother curve after that value. It should be pointed out that the coefficient C_L^- is very sensitive to the grid discretization at the gap. A better agreement is obtained for a discretization of 40 cells per diameter, reducing, for example, for *e/D*=0.125, the differences between numerical and experimental results from around 60% to 50%.

Jarno-Druaux explains the variation of force coefficients with the gap-diameter separating in three regimes: a first for *e/D* between 0.04 and 0.25, a second region for *e/D* between 0.25 and 1.0, and a third region for *e/D* larger than 1.0.

In the first regime, a jet flow on the gap–side of the cylinder appears and two upper attached vortices are developed. In the second region, the influence of the wall is different, the jet flows are suppressed and the velocity of the flow through the bottom at the gap is accelerated. In the third regime the wall does not have an influence on the coefficients.

In order to compare the flow regime obtained with the numerical model and with the experimental tests, Figure 10 (a) and (b) show the streamlines in the cylinder vicinity for *t/T*=0.22 and *t/T*=0.33 respectively for *e/D* equal to 0.09 and 0.5. Figure 10 (c) and (d) shows the vorticity field and the streamlines obtained with the numerical model. In this analysis *t/T*=0 correspond to the instant when a crest is above the cylinder as can be seen in the free surface elevation represented in Figure 9.

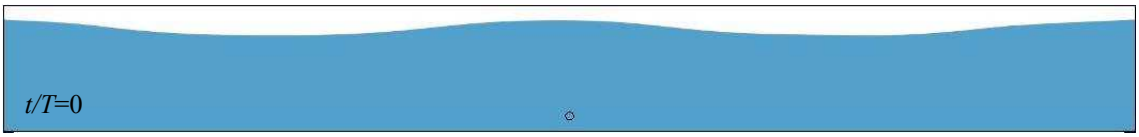

Figure 9. Free surface elevation in the numerical flume – instant when a crest is above the cylinder (*t/T*=0)

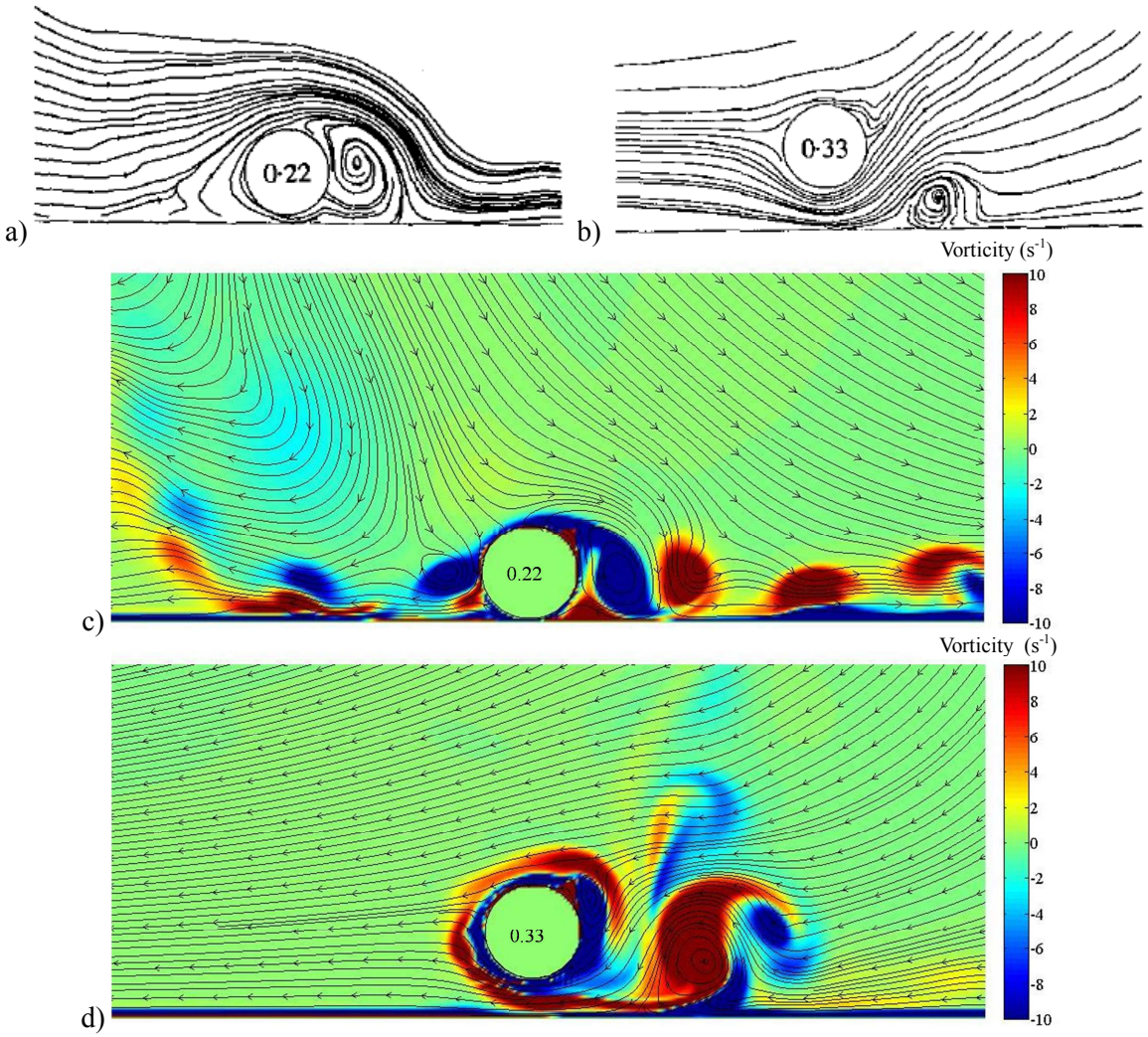

Figure 10. Experimental streamline at *t/T* 0.22 and 0.33 for *e/D*=0.09 (a) and *e/D*=0.5 (b) and the correspondent streamline and vorticity field at *t/T* for *e/D*=0.09 (c) and *e/D*=0.5 (d)

For *e/D*=0.09, first regime, the experimental tests show one major attached vortex forming on the outward side of the cylinder per each half-period. While these vortices are vanishing, another small vortex develops on the other side of the cylinder issuing from the gap-side. Even though the streamline pattern obtained with the numerical model is similar to the experimental one (see Figure 10 a) and c)), in the numerical case, the major vortices take longer to vanish and with the flow reversal, each of them go around the cylinder and shed in the wake of the cylinder. This difference can probably be due the fact that the numerical value of *e/D* is not exactly 0.09 taking the value of 0.09375 and because of that the vortices regime is different. In opposition to the experimental case, in the numerical case the small vortices do not issue from the gap-side for every half period. This difference is probably due to the scarce number of cells at the gap (three in this case).

For *e/D*=0.5, second regime, the experimental tests show that the major vortex forming, one each half period, are those issuing from the gap-side of the cylinder and are shed and convected toward the wall. For this gap, the streamline pattern obtained for the numerical model is very similar to the observed at the experimental test (Figure 10 (b) and (d)) showing the same vortex formation.

These results elucidate the agreement observed for the trend on the variation of the drag, inertia and lift coefficients with the *e/D* between numerical and experimental results.

5. Conclusions

This paper presents the application of IH-2VOF for study the wave interacting with a submarine outfall schematically represented by a circular cylinder. Numerical simulations were carried out for a water depth, h=0.27 m, a wave period, T, of 1.08 s and a wave height, H, of 0.047 m, corresponding to the conditions used in the experimental work of Jarno-Druaux *et al*. (1995).

The study includes analyses of convergence with the mesh discretization in order to define the best grid dimension in the vicinity of the cylinder, i.e., the number of cells that represents a good compromise between computational time and accuracy of the results. The grid dimension chosen for the simulations was the coarser for which convergence was obtained, corresponding to the case of 32 cells for cylinder diameter, where the differences from the more refined mesh simulation less than 12% for the in-line forces and less than 10% for the transverse forces

To study the influence of the wall proximity in the cylinder forces, numerical simulations were carried out for 15 cases with ratios between the pipe distance from the bottom, e, and the pipe diameter, D, varying from 0.0625 to 1.5. The results of the lift, drag and inertia coefficients were compared with the experimental results and the same trend in the variation with the increase of the gap between the cylinder and the bottom was obtained for numerical and experimental results. However, some differences could be observed. Generally, the numerical model gives larger values of the coefficients than the experimental ones with differences of: from 30 to 70% for the drag coefficient, 25% for the inertia coefficient and around 10% for the lift coefficient directed away from the bottom wall and up to 30% in the opposite direction. The differences between numerical and experimental drag coefficient could be explain by differences on the interference region of both bottom and cylinder boundary layer, since the influence of the wall depends on whether the cylinder is or is not immersed in that layer, especially important for small e/D. Another possible reason is that different wave height above the cylinder occurred in the experimental and numerical tests. Due to lack of information regarding the velocity profile in a perturbed area and the experimental height above the cylinder, these differences could not be confirmed. Another source of errors, especially important for the lift coefficient directed toward the wall bottom, could be the grid discretization at the gap.

Summarizing, the results obtained for this particular kind of wave-structure interaction show reasonable results, leading to the conclusion that the information obtained could be very useful for development of practical design recommendations.

References

Aristodemo, F., Tomasicchio, G. R., Veltri, P. (2010). New model to determine forces at on-bottom slender pipelines. *Coastal Engineering*, 3, pp. 267-280. Doi:10.1016/j.coastaleng.2010.11.004.

Hsu, T.-J., Sakakiyama, T. and Liu, P.L.-F. (2002) A numerical model for wave motions and turbulence flows in front of a composite breakwater, *Coastal Engineering*, 46, 25-50.

Inverno, J. (2013). Numerical modeling of the interaction between waves and submarine outfalls. Master Thesis, Universidade Nova de Lisboa - FCT, Lisbon (In Portuguese with English abstract).

Jarno-Druaux, A., Sakout, A., Lambert, E. (1995). Interference between a circular cylinder and a plane wall under waves. *Jornal of Fluids and Structures*, 9, pp. 215-230.

Lara, J.L., Garcia, N., Losada, I.J. (2006). RANS modelling applied to random wave interaction with submerged permeable structures. *Coastal Engineering*, 53, pp. 395-417.

Lin, P. and Liu, P.L.-F. (1998). A numerical study of breaking waves in the surf zone, *Journal of Fluid Mechanics*, 359, 239-264.

Losada, I.J., Lara, J.L., Guanche, R., Gonzalez-Ondina, J.M. (2008). Numerical analysis of wave overtopping of rubble mound breakwaters", *Coastal Engineering*, 55(1), 47-62.

Reis, M.T., Neves, M.G. (2003). Structural behaviour of submarine outfalls. Submarine outfalls in Portugal. LNEC Report 24/03 – NPE, Lisbon, January (In Portuguese).

Sumer, B.M., Fredsoe, J. (2006). Hydrodynamics around cylindrical structures (Revised edition). *Advanced Series on Ocean Engineering*, 26, World Scientific, Singapore.